

## Research Article

Justyna Sławińska-Budzich\* and Jacek Mierczyński

# Deformations and stability of granular soils: Classical triaxial tests and numerical results from an incremental model

<https://doi.org/10.2478/sgem-2019-0039>

Received Jul 05, 2019; accepted Jan 10, 2020

**Abstract:** This article presents a modified incremental model describing pre-failure deformations of granular soils under classical triaxial conditions. The original shape of equations has been proposed by Sawicki and Świdziński [40, 41]. A new form of equations that are consistent with the proposed definitions of deviatoric loading and unloading is suggested. Triaxial tests necessary for calibrating the proposed model have been performed. The modified model is used to simulate the deformations and stability of sand for every pre-failure loading path and makes it possible to describe the behaviour of granular soil under both drained and undrained conditions.

A comparison of experimental and numerical results is presented. All investigations were performed in a classical triaxial apparatus.

**Keywords:** constitutive equations, granular soils, deformations, instability, stability

## 1 Introduction

A saturated non-cohesive soil can exhibit features typical of both solid or liquid phases, depending on circumstances or the history of loading. Fully drained or saturated sands can be characterised by parameters typical of solids, such as elasticity, plasticity, high shear strength or viscosity. This kind of behaviour is described by the corresponding constitutive relation, that is, elasticity, plasticity or limit state theory. The classical geotechnical literature

on the modelling of soils and soil–structure interactions within the range of the limit state is rich [e.g. 10, 50].

One of the main aspects of sand modelling is the description of the stress–strain behaviour. The literature presents some simplified methods based on the theory of elasticity, see for example [17]. These methods, however, are insufficient and out of date. Therefore, scientists have begun to develop more sophisticated models such as the theory of elasticity and plasticity [28], hypoplasticity [54] or hyper plasticity, refer to [52, 53]. Many of these models have been developed recently, see for example [1, 19]. Recent studies on deformation modelling and soil stability are described in [6, 7] (bounding surface plasticity); [11, 21] (generalised plasticity); [43–46] (fractional plasticity); [5, 18] (thermomechanical approach); and [20] (Discrete Element Method). However, the bearing capacity of the subsoil is still one of the main problems for engineers and much attention should, therefore, be paid to this issue. The models currently used in geotechnical engineering are usually very comprehensive and numerically extensive. The most popular of them include the Hardening Soil Model, [2], the Cam-Clay Model, [49] or the Nor-Sand Model, [14]. There are also many other models that aim to describe pre-failure soil behaviour, but all of them are still in the development phase.

This article deals with a new approach to the modelling of pre-failure deformations of soils. The basic constitutive equations were first proposed by Sawicki and Świdziński in [30] and further developed in [39–41]. A large set of experimental data for Gdynia sand needed to calibrate the model can be found in [34]. The structure, calibration and predictions of this model, corresponding to complex loading paths for Skarpa sand, are presented in greater detail in [40, 41]. The model describes the behaviour of granular sand, such as deformations or liquefaction, before sand reaches a limit state. Constitutive equations are proposed for an accurate description of the behaviour of sand in two cases: drained (saturated and fully drained) and undrained conditions.

The constitutive equations proposed here have a semi-empirical form. Similar to hypoplasticity, the incremental

\*Corresponding Author: Justyna Sławińska-Budzich: Institute of Hydro-Engineering, Polish Academy of Sciences, Kościarska 7, 80-328 Gdańsk, Poland; Email: stynaju@ibwpan.gda.pl

Jacek Mierczyński: Institute of Hydro-Engineering, Polish Academy of Sciences, Kościarska 7, 80-328 Gdańsk, Poland; Email: mier@ibwpan.gda.pl

model does not rely on ideas associated with elasticity and plasticity (e.g. the yield surface) and does not assume decomposition of deformation into elastic and plastic. The model is based only on the concepts of loading and unloading (which are built into the structure of equations) and on material constants introduced.

The model has a simple mathematical structure and is based on a solid empirical foundation. The set of data used to calibrate the model can be obtained from standard triaxial investigations. Furthermore, the model has the form of several incremental equations and is capable of describing volumetric and deviatoric deformations of granular soil as a function of invariants: mean effective stress and deviator stress. The invariant form of the equations makes it possible to extend the model to 3D conditions, see [31, 35, 36]. A verification of this model based on plane strain tests is presented in [38, 42].

Although the original model gives good predictions for many complex triaxial tests, its authors suggested the algorithmisation of the model and a clear definition of only one form of equations. In the latest version of the Sawicki and Świdziński model [40, 41], predictions sometimes depend on the value of deviator increments and, at other times, on the value of quotient increase. In general, there is no rule when particular equations should be used, and only experimental verification can determine which increase is important. The first attempt to solve this problem was made in [37], but a closed form of the model has not been proposed.

A brief literature review, summarising the development of this model, leads to the conclusion that there is a need to propose one form of general equations that will make it possible to algorithmise this model and thus clearly formulate definitions of deviatoric loading and unloading. This article proposes consistent definitions of deviatoric loading and unloading, one general form of incremental equations, predictions of the model for complex stress paths and application of the algorithmised model to determine the soil stability in Hill's criterion. Experimental tests necessary for the calibration of the model were carried out and base functions were redefined.

## 2 Experimental investigations

### 2.1 Classical triaxial apparatus

The results presented in this article are based on experiments carried out in a classical triaxial apparatus manufactured by GDS Instruments [see 25, 47]. Vertical and lat-

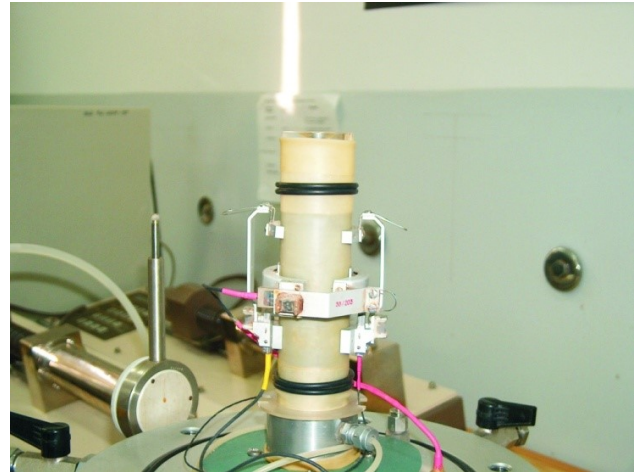


**Figure 1:** Sand sample preparation for testing with gauges installed (photo by W. Świdziński).

eral local displacements are measured by special gauges, which use the Hall effect. The gauges are installed directly on the sand sample. Vertical stress is controlled by moving the table on which the sample is placed, and lateral stresses are applied through the water pressure in the chamber. In the case of saturated or fully drained samples, the pore pressure and volume of water in the sample are read from a pneumatic controller. Figure 1 presents the preparation of a sample for testing.

The whole system for triaxial testing consists of a triaxial chamber, three pressure/volume controllers, an electronic control system and a computer. The apparatus has a Bishop and Wesley chamber [see 3] with a built-in force sensor and a lower load cell, which imposes a vertical load on the sample. The table is moved by increasing the pressure in the lower load cell. With a rigid piston in the upper part of the chamber, a vertical compression force is generated.

The controllers are used for controlling the pressure in the main chamber of the apparatus, for controlling the load in the lower cell and for measuring the pore pressure in the sand sample. They can operate in a pressure change mode or a water volume change mode, so it is possible to perform stress- or strain-controlled tests.

This article presents the results of experiments performed on samples with a diameter of 38 mm and a height of 80 mm. It is important to ensure the homogeneity of the soil sample when it is being formed. The soil samples were prepared in a membrane-lined split moulder. Loose samples were formed by the moist tamping method and dense samples by water pluviation.

All experiments presented in this article were performed on coarse quartz Skarpa sand characterised by the

following parameters: mean particle size  $D_{50} = 0.42$  mm, uniformity coefficient  $U = 2.5$ , minimum void ratio  $e_{\min} = 0.432$ , maximum void ratio  $e_{\max} = 0.677$ , angle of internal friction for loose/dense sand =  $34^\circ/41^\circ$ . In all analyses, the soil mechanics sign convention is applied, in which compression is positive.

### 3 Incremental model and its modification

#### 3.1 Definitions of loading and unloading

The original incremental model proposed by Sawicki and Świdziński [40, 41] has the form of semi-empirical incremental equations and describes the deformation of soils before the limit state is reached. The equations are given as follows:

$$d\varepsilon_v = M dp' + N dq \quad (1)$$

$$d\varepsilon_q = P dp' + Q dq \quad (2)$$

The invariants used in Eqs. (1) and (2) are the following:  $p' = 1/3 (\sigma'_1 + 2\sigma'_3)$ , mean effective stress;  $q = \sigma'_1 - \sigma'_3$ , deviatoric stress;  $\varepsilon_v = \varepsilon_1 + 2\varepsilon_3$ , volumetric strain; and  $\varepsilon_q = 2/3 (\varepsilon_1 - \varepsilon_3)$ , deviatoric strain, where  $\sigma'_1, \varepsilon_1$  are the normal effective vertical stress and vertical strain, respectively, and  $\sigma'_3, \varepsilon_3$  are the normal horizontal effective stress and horizontal strain, respectively.

The functions  $M, N, P, Q$  are determined from analytical approximations of selected experimental results [see 40]. The definitions of loading and unloading assumed in this model are the following:

$$dp' > 0 \text{ is the spherical loading,} \quad (3)$$

$$dp' < 0 \text{ is the spherical unloading,} \quad (4)$$

$$dq > 0 \text{ or } d\eta > 0 \text{ is the deviatoric loading,} \quad (5)$$

$$dq < 0 \text{ or } d\eta < 0 \text{ is the deviatoric unloading} \quad (6)$$

where  $\eta$  is a dimensionless stress ratio defined as

$$\eta = \frac{q}{p'} \quad (7)$$

In Sawicki's original model, the signs of  $dq$  or  $d\eta$  determine whether loading or unloading is applied (Eqs. 5 and 6), but this generally leads to contradictions. One has to consider the sign of  $d\eta$ , because the information on the

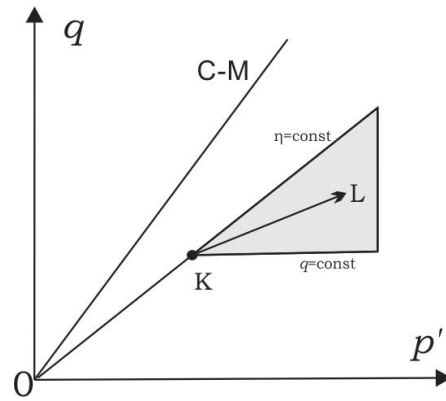


Figure 2: The stress plane  $p' - q$  with a grey zone in which the definitions of deviatoric loading and unloading are unclear.

sign of  $dq$  is not sufficient to clearly determine whether loading or unloading is applied, which is shown by predictions for stress paths for  $q = const$ . Therefore, to definite deviatoric loading and unloading, it was necessary to include a condition in which the sign of  $d\eta$  is specified. When this fact is taken into account, the model gives good predictions of soil deformations corresponding to the stress path for  $q = const$  or stress paths characteristic of the liquefaction phenomenon [see 41]. However, such definitions lead to some contradictions, and there is a part of the stress plane in which whether the case considered represents deviatoric loading or unloading is unknown. To prove it, let us consider a stress path originating at a point K in the  $p' - q$  space located within the grey zone in Figure 2 – for example, the path KL. It is evident that the path KL can be described by conditions  $dq > 0$  and  $d\eta < 0$ . Therefore, in this case, conditions (5) and (6) are unclear, and the kind of loading cannot be clearly defined. Consequently, it is unclear how precisely to build equations (1) and (2). In Sawicki's model, this problem is solved experimentally. It is simply checked, which sign ( $dq$  or  $d\eta$ ) results in a better prediction. However, with this approach, the model still cannot be algorithmised, and, therefore, the present authors propose new definitions of deviatoric loading and unloading and, hence, a modification of the main equations.

The revised definitions have the following forms:

$$dp' > 0 \text{ is the spherical loading,} \quad (8)$$

$$dp' < 0 \text{ is the spherical unloading,} \quad (9)$$

$$d\eta > 0 \text{ is the deviatoric loading,} \quad (10)$$

$$d\eta < 0 \text{ is the deviatoric unloading,} \quad (11)$$

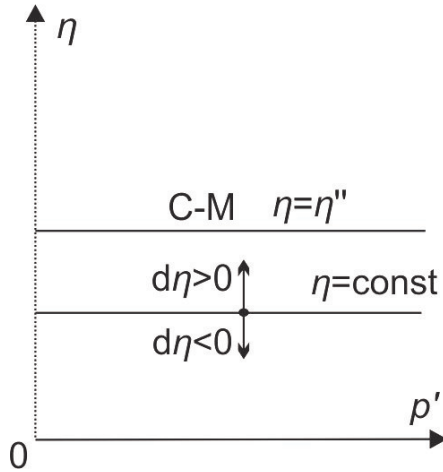


Figure 3: The meaning of the variable  $\eta$  and the sign of  $d\eta$ .

The definitions of spherical loading and unloading are the same as in the previous case (Eqs. 3 and 4), whereas the definitions of deviatoric loading and unloading are modified and only the sign of  $d\eta$  is considered. Thus, the incremental equations have the following forms:

$$d\varepsilon_v = Md p' + Nd\eta \quad (12)$$

$$d\varepsilon_q = Pd p' + Qd\eta \quad (13)$$

The functions  $M, N, P, Q$  are determined from analytical approximations of selected experimental results. However, their forms are different from those of  $M, N, P, Q$  in Eqs. (1) and (2). The basic stress paths that are needed to determine these functions are different too.

To illustrate the physical meaning of the variable  $\eta$ , the possible directions and signs of its increments are shown in the  $p' - \eta$  plane in Figure 3. The proposed incremental equations (12) and (13) are built based on the  $p'$  and  $\eta$  invariants, and, therefore, this space is used in the description. When the stress path is defined by the condition  $d\eta > 0$ , the soil is approaching the limit state. The condition  $d\eta < 0$  means that the soil is 'moving away' from collapse, whereas at a constant  $\eta$ , the soil is stable.

### 3.2 Units used in the model

The following units are adopted in the model:  $10^5 \text{ N/m}^2$ , corresponding to 100 kPa, for stress and  $10^{-3}$ , corresponding to 0.1%, for strain. The values of all stresses and strains used in the proposed model follow this convention, and the experimental data are presented in these units.

### 3.3 Calibration of the model

In the modified equations, the functions  $M, P$  correspond to deformations for the stress paths  $\eta = \text{const}$ , whereas the functions  $N, Q$  correspond to deformations for  $p' = \text{const}$ . In each of the functions  $M, N, P, Q$ , a distinction has to be made regarding the sign of  $dp'$  and  $d\eta$ , which results in two types of each function. The upper indices  $l$  and  $u$  correspond, respectively, to loading and unloading. The definitions of these functions are the following:

$$M^l = \frac{\partial \varepsilon_v^{OA}}{\partial p'}, \quad M^u = \frac{\partial \varepsilon_v^{AO}}{\partial p'} \quad (14)$$

$$N^l = \frac{\partial \varepsilon_v^{AB}}{\partial \eta}, \quad N^u = \frac{\partial \varepsilon_v^{BA}}{\partial \eta} \quad (15)$$

$$P^l = \frac{\partial \varepsilon_q^{OA}}{\partial p'}, \quad P^u = \frac{\partial \varepsilon_q^{AO}}{\partial p'} \quad (16)$$

$$Q^l = \frac{\partial \varepsilon_q^{AB}}{\partial \eta}, \quad Q^u = \frac{\partial \varepsilon_q^{BA}}{\partial \eta} \quad (17)$$

To effectively describe the results of experiments and to determine the functions  $M, N, P, Q$ , the idea of a 'common' curve is adopted, see [40]. To obtain the functions  $M, P$ , a series of experiments for different slopes of the stress paths OA and AO are conducted by the authors. The experiments are performed for two cases, namely, for contractive and dilative 'Skarpa' sands. Both these states of soil are defined by the position with respect to the steady-state line, see [40].

#### 3.3.1 Functions for contractive sand

To investigate the behaviour of contractive soil and to determine volumetric and deviatoric strains, experiments in a triaxial apparatus are performed for a set of different stress paths for  $\eta = \text{const}$ . Each test consists of two phases. In the first stage, the soil sample is subjected to anisotropic compression through the confining pressure, so, in this case, the mean effective stress  $p'$  increases, and the specimen is subjected to pure spherical loading (OA path). In the second phase, a return path is applied, with the same value  $\eta = \text{const}$  and a decreasing  $p'$  (AO path). Therefore, the sample is subjected to pure spherical unloading. In this way, the soil behaviour during single loading–unloading loop is tested. Thus a series of experiments are performed to analytically determine the functions  $M^l, P^l, M^u, P^u$  describing the behaviour of volumetric and deviatoric strains.



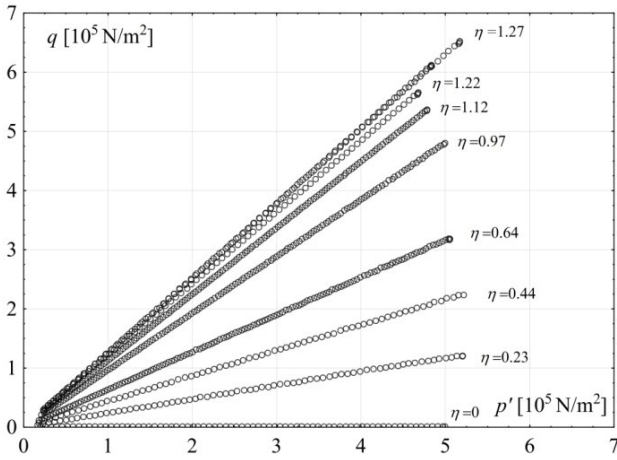


**Figure 4:** Stress paths  $\eta = const$  used for the calibration of the incremental model.

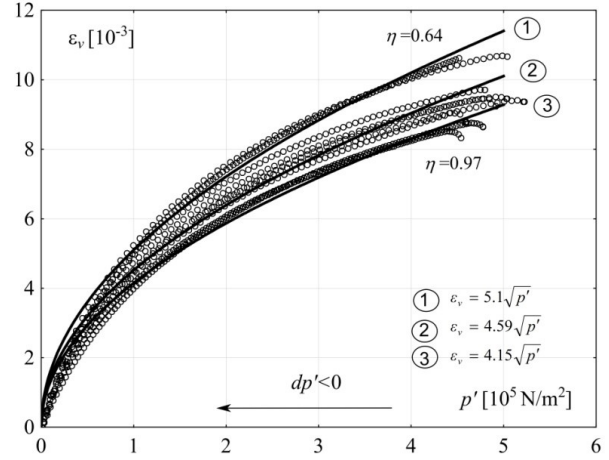


**Figure 6:** Experimental results and an approximation curve for volumetric strain that develops in contractive sand for various stress paths  $\eta = const$  when  $dp' < 0$ .

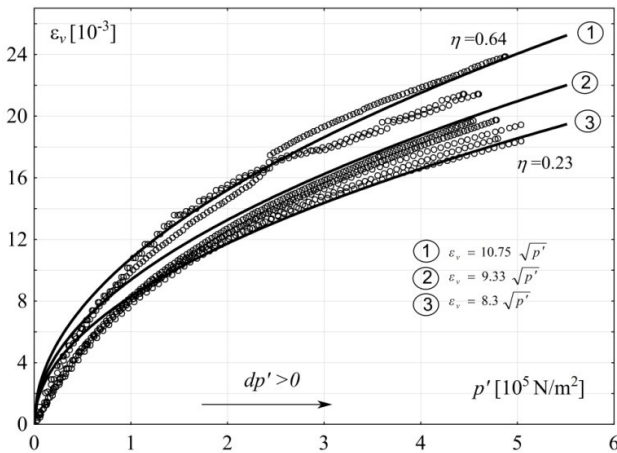


**Figure 5:** Experimental results and an approximation curve for volumetric strain that develops during anisotropic consolidation of contractive sand.

**Table 1:** List of experiments performed on contractive sand samples and the corresponding results for a single spherical loading–unloading loop.

| Test   | $\eta = const$ | $dp' > 0$ |         | $dp' < 0$ |         |
|--------|----------------|-----------|---------|-----------|---------|
|        |                | $I_D^0$   | $A_v^u$ | $I_D^0$   | $A_v^l$ |
| LH75d  | $\eta = 0.64$  | 0.077     | 10.75   | 0.239     | 5.10    |
| LH77d  | $\eta = 0.97$  | 0.146     | 8.82    | 0.280     | 4.15    |
| LH79d  | $\eta = 0.44$  | 0.23      | 8.69    | 0.356     | 5.07    |
| LH80d  | $\eta = 1.12$  | 0.113     | 9.02    | 0.248     | 4.17    |
| LH81d  | $\eta = 1.27$  | 0.082     | 10.26   | 0.204     | 4.49    |
| LH81dd | $\eta = 1.22$  | 0.057     | 10.42   | 0.201     | 4.45    |
| LH82d  | $\eta = 0.23$  | 0.094     | 8.3     | 0.181     | 4.54    |
| LH84d  | $\eta = 0$     | 0.056     | 8.4     | 0.178     | 4.72    |

Figure 4 shows the stress paths tested. Figure 5 shows the development of volumetric strain corresponding to contractive soil behaviour for each stress path in Figure 4 for spherical loading paths. Figure 6 shows the development of volumetric strain for spherical unloading paths. Table 1 presents a list of experiments performed on contractive sand samples and their results for a single spherical loading–unloading loop.  $I_D^0$  denotes the initial index of density of each phase.  $A_v$ ,  $A_v^u$  are coefficients needed to determine the functions  $M^l$  and  $M^u$ . Each test is numbered and corresponds to a selected stress path  $\eta = const$ . The least squares method is used for all approximations of baseline tests in this article.

Figure 5 shows the experimental results and an analytical fit. An analytical approximation of these curves can be described using the following formula:

$$\epsilon_v = A_v \sqrt{p'} = 9.33 \sqrt{p'} \quad (18)$$

According to definition (14),

$$M^l = \frac{\partial \epsilon_v^{0A}}{\partial p'} = \frac{A_v}{2\sqrt{p'}} = \frac{9.33}{2\sqrt{p'}} \quad (19)$$

Numbers 1 and 3 in Figure 5 denote a limit and an analytical approximation of experimental results, and number 2 denotes an averaged approximation of all approximations, whose equations for each test are given in Table 1. The limit values of the coefficient  $A_v$  are 8.3 and 10.75, whereas the average value is 9.33. In order to formulate the function  $M^l$ , it was assumed that its character does not depend on the value of  $\eta$ .

Similarly, analytical approximations corresponding to spherical unloading are presented in Figure 6 and de-

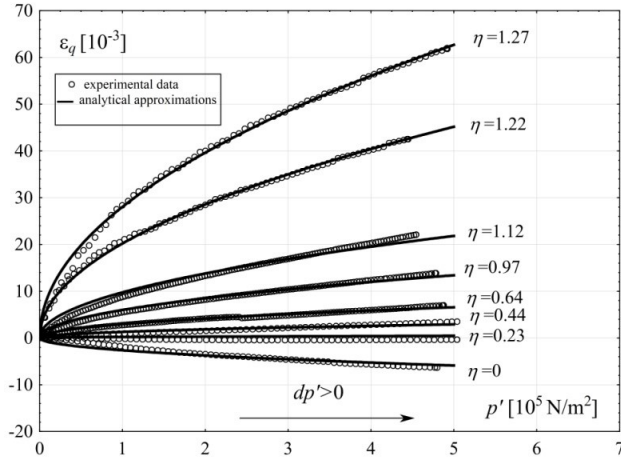


**Figure 7:** Experimental results and an approximation of deviatoric strain that develops in contractive sand for stress paths  $\eta = const$  when  $dp' > 0$ .

scribed in detail in Table 1. The boundary values of the coefficient  $A_v^u$  are 5.1 and 4.15, whereas the average value is 4.59. Therefore, when creating the function  $M^u$ , it was assumed that its character does not depend on the value of  $\eta$ .

The averaged approximation is

$$\varepsilon_v = A_v^u \sqrt{p'} = 4.59 \sqrt{p'} \quad (20)$$

According to definition (14),

$$M^u = \frac{\partial \varepsilon_v^{AO}}{\partial p'} = \frac{A_v^u}{2\sqrt{p'}} = \frac{4.59}{2\sqrt{p'}} \quad (21)$$

To determine the functions  $P^l$  and  $P^u$ , it is necessary to introduce a ‘common’ curve to approximate experimental results describing the development of deviatoric strains. To determine the function  $P^l$  for the set of experimental results presented in Figure 7, the following steps need to be performed. An analytical approximation of the experimental data can be defined using the following formula:

$$\varepsilon_q = A_q \sqrt{p'} \quad (22)$$

Figure 7 shows that each stress–strain relation can be approximated with very good accuracy. The data presented correspond to stress paths given in Figure 6. In Figure 7, on the right side of each set of experimental data, the corresponding  $\eta$  value is shown. Table 2 presents the values of the parameter  $A_q$  corresponding to the selected stress path and the initial relative density of soil samples.

The coefficient  $A_q$  (similar to the coefficient  $A_v$  for volumetric strain) represents the magnitude of deviatoric strain for a given stress path  $\eta = const$ . The higher the value of  $A_q$ , the greater the value of deviatoric strain for

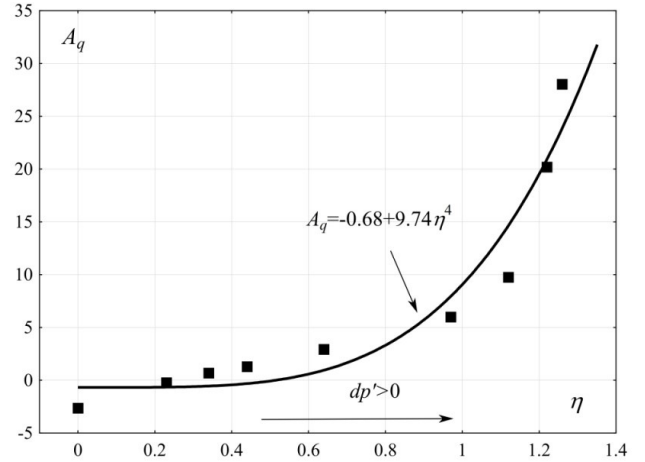


**Figure 8:** Relationship  $A_q(\eta)$ : experimental results and their analytical approximation for deviatoric strain that develops in contractive sand for stress paths  $\eta = const$  when  $dp' > 0$ .

**Table 2:** Series of experiments performed to calibrate the model for contractive sand.

| Test   | $\eta = const$ | First phase: $dp' > 0$ |       |
|--------|----------------|------------------------|-------|
|        |                | $I_D^0$                | $A_q$ |
| LH75d  | $\eta = 0.64$  | 0.077                  | 2.94  |
| LH77d  | $\eta = 0.97$  | 0.146                  | 6     |
| LH79d  | $\eta = 0.44$  | 0.23                   | 1.3   |
| LH80d  | $\eta = 1.12$  | 0.113                  | 9.76  |
| LH81d  | $\eta = 1.27$  | 0.082                  | 28.3  |
| LH81dd | $\eta = 1.22$  | 0.057                  | 20.2  |
| LH82d  | $\eta = 0.23$  | 0.094                  | 0.21  |
| LH84d  | $\eta = 0$     | 0.056                  | -2.63 |

the corresponding anisotropic stress path and for a given value of the mean effective stress  $p'$ . The greatest value of  $A_q = 28.3$  corresponds to the stress path  $\eta = 1.27$ , whereas the smallest  $A_q = -2.63$  corresponds to the stress path  $\eta = 0$ . Figure 7 and Table 2 present that the value of the coefficient  $A_q$  increases monotonically with an increasing value of  $\eta$ .

Figure 8 presents the function  $A_q(\eta)$  obtained from experimental data and its analytical approximation.  $A_q(\eta)$  is given using the following formula:

$$A_q = a + b\eta^4 = -0.68 + 9.74\eta^4 \quad (23)$$

On the basis of Eqs. (22) and (23), the final averaged approximation has the following form:

$$\begin{aligned} \varepsilon_q &= A_q \sqrt{p'} = (a + b\eta^4) \sqrt{p'} \\ &= (-0.68 + 9.74\eta^4) \sqrt{p'} \end{aligned} \quad (24)$$

**Table 3:** List of experiments performed on contractive sand samples and the corresponding results for a single spherical loading–unloading loop.

| Test  | $\eta = const$ | First phase: |       |       | Second phase: $dp' < 0$ |         |
|-------|----------------|--------------|-------|-------|-------------------------|---------|
|       |                | $I_D^0$      | $A_v$ | $A_q$ | $I_D^0$                 | $A_v^u$ |
| SH73d | $\eta = 0.96$  | 0.702        | 3.3   | 1     | 0.749                   | 2.59    |
| SH75d | $\eta = 1.23$  | 0.701        | 3.28  | 2.22  | 0.749                   | 3.04    |
| SH76d | $\eta = 0.64$  | 0.669        | 3.72  | 0.52  | 0.722                   | 3.04    |
| SH77d | $\eta = 0.34$  | 0.703        | 3.52  | 0.62  | 0.753                   | 2.9     |
| SH78d | $\eta = 0$     | 0.701        | 3.45  | 0     | 0.750                   | 2.96    |
| SH80d | $\eta = 1.35$  | 0.632        | 3.27  | 6.5   | 0.678                   | 3.35    |

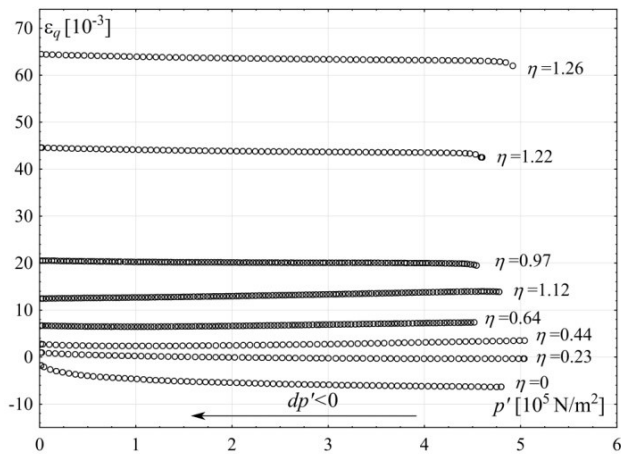


**Figure 9:** Experimental results for deviatoric strain that develops in contractive for stress paths  $\eta = const$  when  $dp' < 0$ .

The curve described using Eq. (24) is a ‘common’ curve containing information about the behaviour of deviatoric strain for every anisotropic consolidation test. Despite the complex behaviour of soil in this case, the approximation contains only two coefficients:  $a$  and  $b$ .

According to definition (16), the function  $P^l$  is defined as

$$P^l = \frac{(a + b\eta^4)}{2\sqrt{p'}} = \frac{(-0.68 + 9.74\eta^4)}{2\sqrt{p'}} \quad (25)$$

To determine the function  $P^u$ , it is necessary to analyse the experimental results given in Figure 9, where  $\eta = const$ . The case considered is spherical unloading. The function  $P^u$  describes deviatoric strains, so according to (17), for such a case,

$$P^u = 0 \quad (26)$$

It indicates that there is no change in deviatoric strain during spherical unloading for stress  $\eta = const$ .

The results of experiments needed to determine the functions  $N^l$ ,  $N^u$ ,  $Q^l$ ,  $Q^u$  are presented in [40]. However,

the form of these functions is different from that in the original model. According to Eqs. (15) and (17), the functions for contractive Skarpa sand are given as follows:

$$N^l = 4c_1\eta^4\sqrt{p'}, \quad c_1 = 2.97; \quad (27)$$

$$N^u = a_v\sqrt{p'}, \quad a_v = -0.87; \quad (28)$$

$$Q^l = b_1b_2\exp(b_2\eta)\sqrt{p'}, \quad (29)$$

$$b_1 = 0.023, \quad b_2 = 6.245$$

$$Q^u = b_q\sqrt{p'}, \quad b_q = 0.76. \quad (30)$$

### 3.3.2 Functions for dilative sand

Similar to contractive sand, a series of experiments are performed to determine the ‘basic functions’ for dilative sand. The qualitative character of the functions  $M^l$ ,  $M^u$ ,  $P^l$ ,  $P^u$  is the same as in the previous case, but their quantitative nature is different. Table 3 lists and describes all experiments performed on dilative sand samples.  $I_D^0$  denotes the initial relative density of each phase.  $A_v$  and  $A_v^u$  are coefficients needed to determine the functions and  $M^u$ . Each test is numbered and corresponds to a different stress path  $\eta = const$ .

For the case considered, the average values of the parameters  $A_v$  and  $A_v^u$  are 3.42 and 2.98, respectively. The following functions  $M^l$ ,  $M^u$  can be presented (similarly as for the contractive sand):

$$M^l = \frac{A_v}{2\sqrt{p'}} = \frac{3.42}{2\sqrt{p'}} \quad (31)$$

$$M^u = \frac{A_v^u}{2\sqrt{p'}} = \frac{2.98}{2\sqrt{p'}} \quad (32)$$

In this case as well, the coefficient  $A_q$  is a monotonic function of  $\eta$ , see Figure 10.

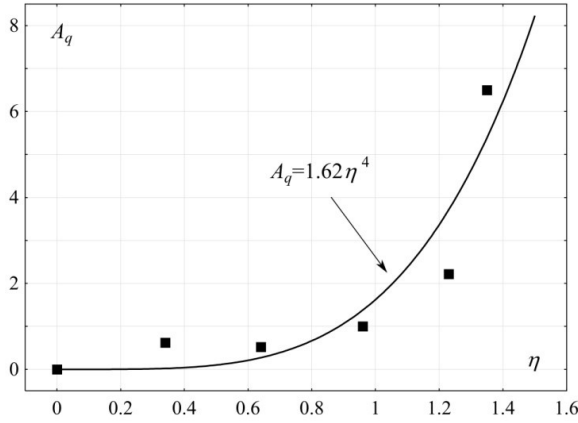


**Figure 10:** Relationship  $A_q(\eta)$ : experimental results and their analytical approximation for deviatoric strain that develops in dilative sand for stress paths  $\eta = const$  when  $dp' > 0$ .

Similar to that for the contractive sand, it can be seen that the higher the value of  $A_q$ , the greater the value of deviatoric strain for the corresponding anisotropic stress path and a given value of the mean effective stress  $p'$ . The greatest value of corresponds to the stress path and the smallest value ( $A_q = 0$ ) corresponds to the stress path  $\eta = 0$ . Figure 10 and Table 3 show that the value of the coefficient increases monotonically with an increase in the value of  $\eta$ . Figure 10 presents the function obtained from experimental data. An analytical approximation of this function is given by

$$A_q = b\eta^4 = 1.62\eta^4. \quad (33)$$

On the basis of Eqs. (22) and (23), the final averaged approximation is written as follows:

$$\varepsilon_q = A_q \sqrt{p'} = b\eta^4 \sqrt{p'} = 1.62\eta^4 \sqrt{p'}. \quad (34)$$

The curve defined using Eq. (34) is a ‘common’ curve containing information about the development of deviatoric strain for every anisotropic consolidation test. Despite the complex response of soil in this case, the approximation function has only one coefficient  $b$ .

According to definition (16), the function  $P^l$  is

$$P^l = \frac{b\eta^4}{2\sqrt{p'}} = \frac{1.62\eta^4}{2\sqrt{p'}}. \quad (35)$$

The experimental results show that deviatoric strain does not develop in dilative sand for stress paths  $\eta = const$  when  $dp' < 0$ . Therefore,

$$P^u = 0. \quad (36)$$

The experiments needed to determine the functions  $N^u$ ,  $Q^l$ ,  $Q^u$  for dilative sand are presented (similar to those for

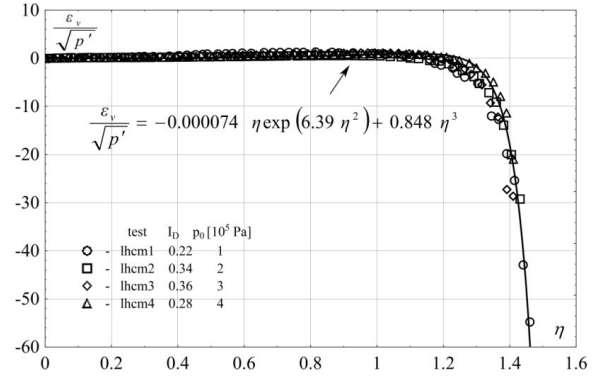


**Figure 11:** Experimental results for pure shearing of dilative sand presented in the form of a single ‘common’ curve.

the contractive sand) in [40]. However, the form of these functions is different from that original model. According to Eqs. (15) and (17), the functions for dilative Skarpa sand are given as follow:

$$N^l = 4c_1\eta^4 \sqrt{p'}, \quad c_1 = 2.97; \quad (37)$$

$$N^u = a_v \sqrt{p'}, \quad a_v = -0.39; \quad (38)$$

$$Q^l = b_1 b_2 \exp(b_2 \eta) \sqrt{p'}, \quad (39)$$

$$b_1 = 0.00035, \quad b_2 = 6.648;$$

$$Q^u = b_q \sqrt{p'}, \quad b_q = 0.4. \quad (40)$$

An approximation of the experimental results for volumetric strain needed to determine the function  $N^l$  in [40] is given as follows:

$$\frac{\varepsilon_v}{\sqrt{p'}} = \begin{cases} a_1 \eta^2 + a_2 \eta & \text{for } 0 \leq \eta \leq \eta' \\ (a_3 \eta^2 + a_4 \eta + a_5) (\exp(a_6 \eta) - 1) & \\ \text{for } \eta' \leq \eta \leq \eta'' & \end{cases} \quad (41)$$

However, approximation (41) is too complex and contains six coefficients. Therefore, a simplified function proposed by the present authors has the following form:

$$\frac{\varepsilon_v}{\sqrt{p'}} = a_1 \exp(a_2 \eta^2) + a_3 \eta^3. \quad (42)$$

Figure 11 presents the experimental results for pure shearing of dilative sand in the form of a single ‘common’ curve. The function given by Eq. (42) has a simpler form than Eq. (41), as it is characterised by only three coefficients.

It should be noted that the behaviour of dilative sand during pure shearing is different from that of contractive



**Table 4:** Functions needed to build the incremental model.

|       | Function              |  | Average values of coefficients |   |
|-------|-----------------------|--|--------------------------------|---|
|       | Contractive           | Dilative   | Contractive                    | Dilative  |
| $M^l$ |                       | $A_v / 2\sqrt{p'}$                               | $A_v = 9.33$                   | $A_v = 3.48$  |
| $P^l$ |                       | $(a + b\eta^4) / 2\sqrt{p'}$                     | $a = -0.68$<br>$b = 9.74$      | $a = 0$<br>$b = 1.62$   |
| $N^l$ | $4c_1\eta^3\sqrt{p'}$ | $(2a_1a_2\exp(a_2\eta^2) + 3a_3\eta^2)\sqrt{p'}$ | $c_1 = 2.97$                   | $a_1 = -0.74 \times 10^{-4}$<br>$a_2 = 6.39$<br>$a_3 = 0.848$ |
| $Q^l$ |                       | $b_1b_2(\exp b_2\eta)\sqrt{p'}$                  | $b_1 = 0.023$<br>$b_2 = 6.245$ | $b_1 = 3.5 \times 10^{-4}$<br>$b_2 = 6.648$                   |
| $M^u$ |                       | $A_v^u / 2\sqrt{p'}$                             | $A_v^u = 4.59$                 | $A_u^v = 3$   |
| $P^u$ |                       | 0  | -                              | -   |
| $N^u$ |                       | $a_v\sqrt{p'}$                                   | $a_v = -0.87$                  | $a_v = -0.39$   |
| $Q^u$ |                       | $b_q\sqrt{p'}$                                   | $b_q = 0.76$                   | $b_q = 0.4$   |

sand. For contractive sand, volumetric strain increases in all stages of pure shearing until the sample is destroyed. For dilative sand, volumetric strain increases slightly and then, when the dimensionless stress  $\eta$  reaches  $\eta'$ , it begins to decrease rapidly. Hence, the function  $N^l$  for dilative sand is qualitatively different from that for contractive sand (see Eq. 15) and has the following form:

$$N^l = (2a_1a_2\exp(a_2\eta^2) + 3a_3\eta^2)\sqrt{p'}, \quad (43)$$

$$a_1 = -0.000074, a_2 = 6.39, a_3 = 0.848.$$

### 3.4 Modified model: Summary

Strains corresponding to any stress path are defined using Eqs. (12) and (13). The information regarding the state of soil (contractive or dilative) is required to use the appropriate set of the functions  $M, N, P, Q$ . Table 4 presents all modified functions necessary to build Eqs. (12) and (13). Predictions for complex tests (other than basic stress paths) are always a combination of approximations of the designated  $M, N, P, Q$  in accordance with Eqs. (12) and (13).

Let us consider any point  $V_0$  in the  $p' - \eta$  plane and draw two lines  $p' = const$  and  $\eta = const$  running through this point. The plane  $p' - \eta$  will thus be divided into four regions, see Figure 12. Any stress path starting at the point  $V_0$  can be located in one of the regions delimited by the lines  $p' = const$  or  $\eta = const$ . Depending on the region in which it is located, appropriate functions will be used to build Eqs. (12) and (13). In this simple way, the complex behaviour of soil can be described for every linear loading path, focusing especially on deformations, as shown

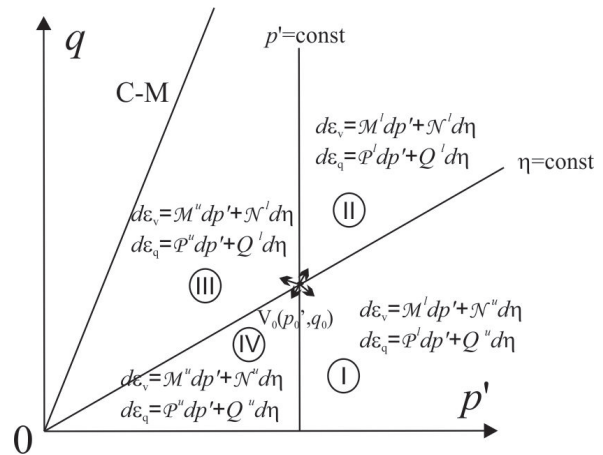


**Figure 12:** Diagram illustrating the application of subsequent incremental equations.

in Figure 12, on stability. The forms of base functions and appropriate coefficients are presented in Table 4.

## 4 Soil stability

In soil mechanics, the loss of stability is defined as a sudden impossibility of transferring loads through the soil, which takes place, for example, during liquefaction. Some literatures describe the differences between instability and strain softening [e.g. 4, 22]. Strain softening can be defined as a rapid increase in deformation caused by a small load change occurring in a very short time. The problem of soil stability is discussed in many publications, where it is defined by Hill's criterion, [8, 9, 24, 27]. Hill's criterion de-

finishes the stability by the sign of the second-order work:

$$d^2W = d\sigma d\varepsilon, \quad (44)$$

assuming that stable material fulfils the condition

$$d^2W > 0. \quad (45)$$

For a triaxial configuration, expression (44) takes the following form:

$$d^2W = d\sigma_1 d\varepsilon_1 + 2d\sigma_3 d\varepsilon_3 = d\varepsilon_v dp + d\varepsilon_q dq \quad (46)$$

Incorporating Eqs. (12) and (13) into (46), the following form can be obtained:

$$d^2W = \left(M - \frac{\eta}{p}N\right) (dp)^2 + \left(\frac{1}{p}N + P - \frac{\eta}{p}Q\right) dpdq + \frac{1}{p}Q(dq)^2. \quad (47)$$

According to the diagram (in Figure 12), expression (47) can be written as

$$d^2W = \left(M^l - \frac{\eta}{p'}N^u\right) (dp')^2 + \left(\frac{1}{p'}N^u + P^l - \frac{\eta}{p'}Q^u\right) dp'dq + \frac{1}{p'}Q^u(dq)^2, \quad (48)$$

$$d^2W = \left(M^l - \frac{\eta}{p'}N^l\right) (dp')^2 + \left(\frac{1}{p'}N^l + P^l - \frac{\eta}{p'}Q^l\right) dp'dq + \frac{1}{p'}Q^l(dq)^2, \quad (49)$$

$$d^2W = \left(M^u - \frac{\eta}{p'}N^l\right) (dp')^2 + \left(\frac{1}{p'}N^l + P^u - \frac{\eta}{p'}Q^l\right) dp'dq + \frac{1}{p'}Q^l(dq)^2, \quad (50)$$

$$d^2W = \left(M^u - \frac{\eta}{p'}N^u\right) (dp')^2 + \left(\frac{1}{p'}N^u + P^u - \frac{\eta}{p'}Q^u\right) dp'dq + \frac{1}{p'}Q^u(dq)^2. \quad (51)$$

In this way, the stability of Skarpa sand can be discussed for every stress path (before reaching the limit state) as a function of the second-order work.

For example, let us consider region III in the  $p' - q$  plane, and, for simplicity of calculations, let us define a linear stress path originating at the point  $V_0(p'_0, q_0)$  (see Figure 12). Every linear path located within the region is defined as a straight line given by the following equation:

$$q = \alpha p' + \beta, \quad (52)$$

where  $\alpha \in \left[0, \frac{q_0}{p'_0}\right)$ ,  $\beta \in [0, \infty)$ , and for those paths  $d\eta > 0$ ,  $dp' < 0$ .

Using the functions from Table 4 in Eq. (50), the second-order work for contractive sand is given as follows:

$$d^2W = \frac{\Phi(\eta)}{p'\sqrt{p'}} (dp')^2, \quad (53)$$

where

$$\Phi(\eta) = \frac{A_v^u}{2} p' - 4\beta c_1 \eta^3 - \alpha\beta b_1 b_2 \exp(b_2 \eta). \quad (54)$$

Transforming Eq. (52), one obtains the following form:

$$p' = \frac{\beta}{\eta - \alpha}. \quad (55)$$

Introducing Eq. (55) into (54),

$$\begin{aligned} \Phi(\eta) &= \frac{\beta A_v^u}{2(\eta - \alpha)} - 4\beta c_1 \eta^3 - \alpha\beta b_1 b_2 \exp(b_2 \eta) \\ &= \beta \Gamma(\eta), \end{aligned} \quad (56)$$

$$\Gamma(\eta) = \frac{A_v^u}{2(\eta - \alpha)} - 4c_1 \eta^3 - \alpha\beta b_1 b_2 \exp(b_2 \eta). \quad (57)$$

The sign of the second-order work, which is described by expression (53), corresponds to the sign of the function  $\Gamma(\eta)$ . The values of the coefficients are constant, and in this case,  $\beta > 0$ , so the sign of expression (57) depends on the value of  $\alpha$ .

#### 4.1 Deviatoric unloading

To examine the numerical results of the modified model and to show the unstable behaviour of contractive sand under certain conditions, let us consider three experiments performed in a classical triaxial apparatus. Each experiment is conducted in three stages. First, the soil sample is subjected to isotropic consolidation to 200 kPa. Then, each sample is subjected to pure shearing at different levels of deviatoric stress. Finally, deviatoric stress was kept constant, and the mean effective stress is being reduced. Spherical unloading was performed along three different stress paths described using Eq. (52), where  $\alpha = 0.5, 1, 1.5$  and  $\beta = 0$ , see Figure 13.

According to Eqs. (12) and (46), the second-order work for this kind of stress paths has the following form:

$$d^2W = d\varepsilon_v dp' = \frac{(dp')^2}{2\sqrt{p'}} \left(A_v^u - 8c_1 \eta^4\right). \quad (58)$$

Generally, the sign of the function describing the second-order work is the same as the sign of the function

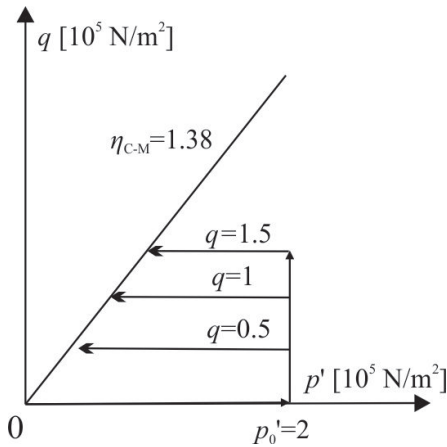


Figure 13: Spherical unloading for different initial deviator stress levels.

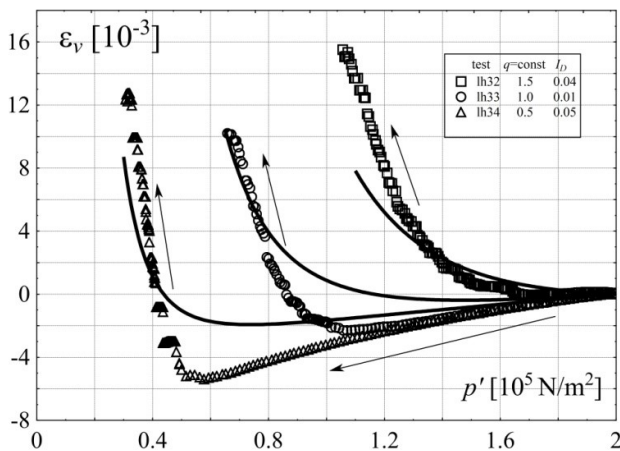


Figure 14: Volumetric strains corresponding to different stress paths.

describing an increase in volumetric strains. The volumetric strains are given by

$$\epsilon_v = \epsilon_v^0 + A_v^u \sqrt{p'} + \frac{8}{7} c_1 q^4 p'^{-3.5}. \quad (59)$$

The experimental results and numerical calculations for average values of the parameters (see Table 4) are presented in Figure 14.

The qualitative agreement with the experimental data is achieved, and the quantitative agreement is sufficient. During the first stage of spherical unloading, dilation takes place and the volume strain decreases. After it reaches the minimum, compaction occurs. The soil loses its stability at the moment when the sign of the volumetric strain increment changes.

The value of  $\eta$  at the moment when changes its sign is given as follows:

$$\eta = \sqrt[4]{\frac{A_v^u}{8c_1}}. \quad (60)$$

For “Skarpa” sand,  $\eta = 0.66$  and, according to Hill’s criterion, when this value is reached, the soil loses stability.

## 4.2 Liquefaction

Saturated soil exhibits traits of a macroscopically solid body. When pore water drainage is prevented, soil can be liquefied, and then it exhibits liquid characteristics. Soil liquefaction is an undesirable phenomenon, often causing catastrophic damage (e.g. buildings sinking in the ground or pipelines being dislodged from the seabed). The phenomenon of liquefaction has been investigated in many monographs, see for example [12, 13, 15, 16, 23, 26, 29, 47].

Undrained conditions can also be investigated in the laboratory, for example, in a triaxial apparatus. First, the sample is isotropically loaded, and then it is sheared under undrained conditions. Only a contractive soil can liquefy. The proposed incremental model can also be used to describe the behaviour of saturated sand under undrained conditions, bearing in mind that liquefied soil behaves like an incompressible body, so it is characterised by a null volumetric strain:

$$d\epsilon_v = M^u dp' + N^l d\eta = 0. \quad (61)$$

After substituting the appropriate functions from Table 4, one obtains

$$d\epsilon_v = \frac{A_v^u}{2\sqrt{p'}} dp' + 4c_1 \eta^3 \sqrt{p'} d\eta = 0. \quad (62)$$

Solving Eq. (62) with the initial condition for  $\eta = 0$ , one obtains the following solution:

$$q = p' \sqrt[4]{\frac{A_v^u}{2c_1} \ln \frac{p'_0}{p'}}. \quad (63)$$

Equation (63) describes the effective stress path leading to liquefaction.

The second-order work defined in terms of stress invariants [see 32] is the following:

$$d^2 W = d\epsilon_v dp' + d\epsilon_q dq, \quad (64)$$

and under undrained conditions ( $d\epsilon_v = 0$ ):

$$d^2 W = d\epsilon_q dq = b_1 b_2 \exp(b_2 \eta) \frac{1}{p'} (dq - \eta dp') dq. \quad (65)$$

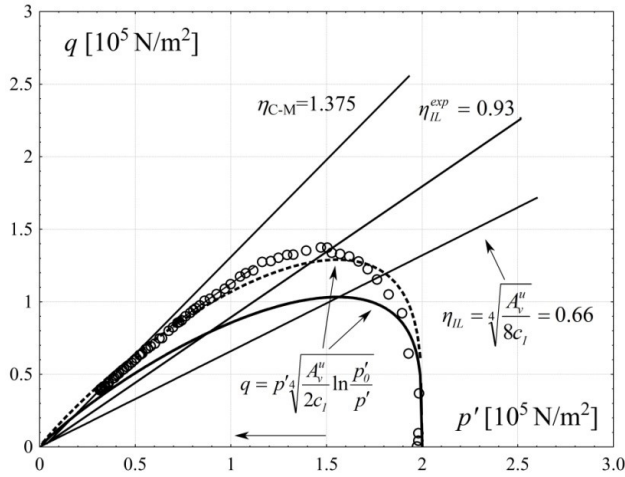


Figure 15: Static liquefaction: experimental and numerical results.

In the first stage of the liquefaction process, the stress deviator increases to the maximum and then begins to decrease. The soil loses its stability when the sign of the deviator changes. Figure 15 shows the liquefaction process: the experimental, see [48], and numerical results for an initial mean effective stress of 200 kPa. The continuous line represents the numerical results (see Eq. 62) for the average values of the coefficients (Table 4), and the dotted line represents the numerical results for slightly modified values of the parameters:  $A_v^u = 6.59$ ,  $c_1 = 1.75$ . The empty dots indicate experimental data. The qualitative agreement with the experimental data is achieved. The quantitative agreement for the slightly altered values of the parameters is good. Changes in all parameter values in the model proposed correspond to the changes described in [33] and their consequences.

The signs of the coefficients  $b_1$ ,  $b_2$  and the increment  $d\eta$  are positive, so expression (65) changes sign when  $dq = 0$ . Figure 15 shows that  $q = const$  only when function (63) reaches an extreme:

$$q_{max} = p' \sqrt[4]{\frac{A_v^u}{8c_1}}. \quad (66)$$

Therefore, the instability line  $\eta_{IL}$  is given by the equation

$$\eta_{IL} = \sqrt[4]{\frac{A_v^u}{8c_1}}, \quad (67)$$

and for the average values of the coefficients,  $\eta_{IL} = 0.66$ .

### 4.3 Behaviour of dilative sand under undrained conditions

The behaviour of sheared dilative sand under undrained conditions is qualitatively different from that of contrac-

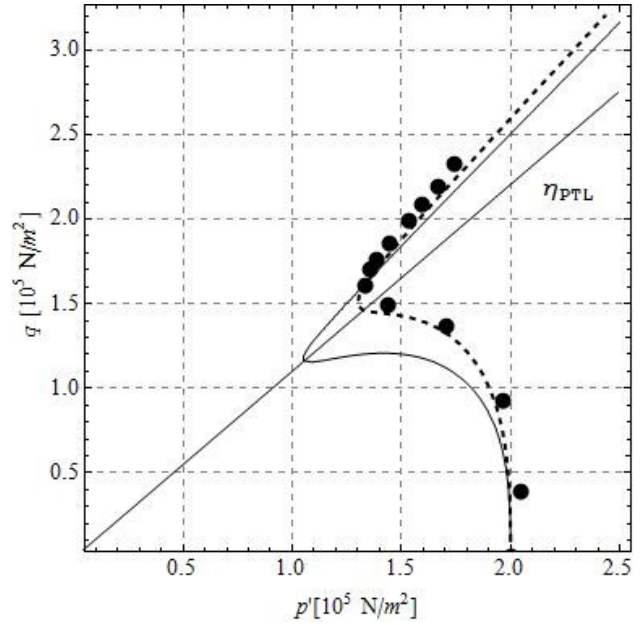


Figure 16: The behaviour of dilative sand under undrained conditions: experimental and numerical results.

tive sand. The mean effective stress  $p'$  decreases to the minimum and then starts to increase. The main general description of stresses is given by Eq. (61), and in the case of dilative sand,

$$d\varepsilon_v = \frac{A_v^u}{2\sqrt{p'}} dp' + \left( 2a_1 a_2 \eta \exp(a_2 \eta^2) + 3a_3 \eta^2 \right) \sqrt{p'} d\eta = 0. \quad (68)$$

The solution of the above equation at the initial condition  $\eta(p'_0) = 0$  is the following:

$$a_1 \eta \exp(a_2 \eta^2) + a_3 \eta^3 = \frac{A_v^u}{2} \ln \left( \frac{p'_0}{p'} \right). \quad (69)$$

Figure 16 shows the experimental and numerical results for an initial mean effective stress of 200 kPa. The continuous line represents the numerical results (see Eq. 69) for the average values of the coefficients (Table 4), whereas the dotted line represents the numerical results for slightly different values of the parameters  $a_2 = 5.8$ ,  $a_3 = 0.6$ . The empty dots indicate experimental data. A satisfactory qualitative agreement with the experimental data is achieved, and the quantitative agreement for the slightly altered values of the parameters is very good.

The equation describing the phase transformation line  $\eta_{PTL}$  is given as follows:

$$\eta_{PTL} = \sqrt[3]{\frac{A_v^u}{3a_3}}. \quad (70)$$

The sign of the second-order work  $d^2W$ , see Eq. (64), is always positive, so, according to Hill's criterion, the soil does not lose stability in this case.

## 5 Conclusions

- a) The semi-empirical model proposed by Sawicki and Świdziński is modified. A new form of equations that are consistent with the proposed definitions of deviatoric loading and unloading is presented. The necessary base functions have been designed and calibrated based on the experiments. In this way, the model is algorithmised and can predict the behaviour of granular soil for every stress path before the limit state is reached.
- b) The modified structure of the equations makes them easier to use them and to determine the second-order work for every stress path, and thus to study the stability of sand under both fully drained and undrained conditions. An example of using the modified model to describe stability in Hill's criterion is presented in the article.
- c) The qualitative agreement between the numerical and experimental results is very good, and the quantitative agreement for slightly changed values of the parameters is also sufficient. Predictions from the model were obtained for drained and undrained conditions.
- d) The model proposed here is based on the analysis of experimental data. The structure of equations is simple, so the model can be used to solve practical problems, especially to describe the liquefaction process or the behaviour of dilative sand under undrained conditions (which is also a novel feature in the modified model).

## References

- [1] Andrianopoulos K. I., Papadimitriou A. G., Bouckovalas G. D. (2010), Bounding surface plasticity model for the seismic liquefaction analysis of geostructures, *Soil Dynamics and Earthquake Engineering*, **30**, 895–911.
- [2] Schanz T., Vermeer P.A., Bonnier P.G. (1999), Formulation and verification of the Hardening-Soil Model, *Beyond 2000 in Computational Geotechnics*, Brinkgreve, ed. Rotterdam: Balkema, 281–290.
- [3] Bishop A. W., Wesley L. D. (1975), A Hydraulic Triaxial Apparatus for Controlled Stress Path Testing, *Geotechnique*, **25** (4), 657–670.
- [4] Chu J., Leong K., (2001), Pre-failure strain softening and pre-failure instability of sand: a comparative study, *Géotechnique*, **51**, 4, 311–321.
- [5] Collins I. F., Kelly P. A. (2002), A thermomechanical analysis of a family of soil models, *Géotechnique*, **52**, 7, 507–518.
- [6] Dafalias Y. F., Manzari M. T., Papadimitriou A. G. (2006), SANICLAY: simple anisotropic clay plasticity model, *Int. J. Numer. Anal. Meth. Geomech.*, **30**, 1231–1257, <https://doi.org/10.1002/nag.524>
- [7] Dafalias Y. F., Taiebat M. (2016), SANISAND-Z: zero elastic range sand plasticity model, *Géotechnique*, **66** (12), 1-15, 10.1680/jgeot.15.P.271
- [8] Daouadji A., AlGali H., Darve F., Zeghloul A. (2010), Instability in Granular Materials: Experimental Evidence of Diffuse Mode of Failure for Loose Sands, ASCE, *Journal of Engineering Mechanics*, ASCE, 136, 5.
- [9] Darve F., Laouafa F., (2000), Instabilities in granular materials and application to landslides, *Mechanics of Cohesive-frictional Materials*, **5**, 8, 627–652.
- [10] Derski W., Izbicki R., Kisiel I., Mróz Z. (1988), *Rock and Soil Mechanics*, PWN/Elsevier, Warszawa/Amsterdam/ Oxford/New York/Tokyo.
- [11] Gajo A., Wood M. (1999), Severn–Trent sand: a kinematic-hardening constitutive model: the  $q-p$  formulation, *Géotechnique*, **49**, 5, 595–614.
- [12] Ishihara K. (1993), Liquefaction and flow failure during earthquakes, *Géotechnique*, **43**, 3, 351–451.
- [13] Ishihara K. (1996), *Soil Behaviour in Earthquake Geotechnics*, Oxford Science Publications, Clarendon Press, Oxford.
- [14] Jefferies M. G., (1993), Nor-Sand: a simple critical state model for sand, *Geotechnique* **43**, 1, 91–103.
- [15] Jefferies M. G., Been K. (2006), *Soil Liquefaction*, Taylor & Francis, London/New York.
- [16] Jefferies M. G., Been K. (2015), *Soil liquefaction: a critical state approach*, Taylor & Francis, Boca Ration/London/New York.
- [17] Hardin, B. O., Blandford, G., E., (1989), Elasticity of particulate materials, *J. Geotech. Engng ASCE*, **115**, 788–805.
- [18] Mitchell, J. K. (1991), Conduction phenomena: from theory to geotechnical practice, *Geotechnique*, **41**, 3, 299 – 340.
- [19] Tasiopoulou P., Gerolymos N., (2015), Constitutive modeling of sand: Formulation of a new plasticity approach, *Soil Dynamics and Earthquake Engineering*, **82**, 205–221.
- [20] Thornton C., Yin K. K. (1991), Impact of elastic spheres with and without adhesion, *Powder Technology*, **65**, 153–166
- [21] Pastor M., Zienkiewicz O. C., Chan A. H. C. (1990), Generalized plasticity and the modelling of soil behaviour, *Int. J. Numer. Anal. Meth. Geomech.*, **14**, 3, 151–190.
- [22] Lade P. V. (1992), Static Instability and Liquefaction of Loose Fine Sandy Slopes, *Journal of Geotechnical Engineering*, **118**, 51–71.
- [23] Lade P. V. and Yamamuro J. A., Eds (1999), *Physics and Mechanics of Soil Liquefaction*, Balkema, Rotterdam/Brookfield.
- [24] Laouafa F., Darve F., (2002), Modelling of slope failure by a material instability mechanism, *Computers and Geotechnics*, **29**, 4, 301–325.
- [25] Menzies B. K. (1988), A computer controlled hydraulic triaxial testing, *Advanced Triaxial Testing of Soil and Rock*, ASTM, 977, Philadelphia, 82–94.
- [26] Mierczyński J. (2014), *The mechanics of liquefied soil*, IBW PAN, Gdańsk, (in Polish).



- [27] Nicot F., Darve F., Huynh Dat Vu Khoa (2007), Bifurcation and second-order work in geomaterials, *International Journal for Numerical and Analytical Methods in Geomechanics*, 31, 1007–1032.
- [28] Pietruszczak S. (2010), *Fundamentals of Plasticity in Geomechanics*, CRC Press, Taylor & Francis Group, Boca Raton/London/New York/Leiden.
- [29] Sawicki A., Świdziński W., (2013), Compaction and liquefaction of a sandy layer: simulation of shaking table experiments, *Archives of Civil Engineering*, LIX, 4.
- [30] Sawicki A. (2007), A study on pre-failure deformations of granular soils, *Archives of Hydro-Engineering and Environmental Mechanics*, 54, 3, 183-206.
- [31] Sawicki A. (2008), 3D and 2D Formulations of Incremental Stress-Strain Relations for Granular Soils, *Archives of Hydro-Engineering and Environmental Mechanics*, 55, 1-2, 45-53.
- [32] Sawicki A. (2012), *The outline of granular soil mechanics*, Wydawnictwo IBW PAN, Gdańsk, (in Polish).
- [33] Sawicki A, Chybicki W. (2009), On accuracy of prediction of pre-failure deformations of granular soils, *Computers & Geotechnics*, 36, 6, 993–999.
- [34] Sawicki A., Mierczyński J., Świdziński W. (2014), Basic set of experiments for determination of mechanical properties of sand, *Bulletin of the Polish Academy of Sciences - Technical Sciences*, 62, 1, 129-137.
- [35] Sawicki A., Sławińska J. (2012a), Deformations and liquefaction of granular soils in plane strain conditions, *Archives of Hydro-Engineering and Environmental Mechanics*, 59, 1-2, 13-35.
- [36] Sawicki A., Sławińska J. (2012b), A study on modelling the plain strain behaviour of sand and its stability, *Archives of Hydro-Engineering and Environmental Mechanics*, 59, 3-4, 85-100.
- [37] Sawicki A., Sławińska J., Mierczyński J. (2014), Structure and calibration of constitutive equations for granular soils, *Studia Geotechnica et Mechanica*, 36, 4, 33-44.
- [38] Sawicki A., Sławińska J., Mierczyński J., Smyczyński M. (2016), Mechanical properties of sand: triaxial versus plane strain investigations. *Archives of Hydro-Engineering and Environmental Mechanics*, 63, 2-3, 135-156.
- [39] Sawicki A., Świdziński W. (2007), Drained Against Undrained Behaviour of Sand, *Archives of Hydro-Engineering and Environmental Mechanics*, 54, 3, 207–222.
- [40] Sawicki A., Świdziński W. (2010a), Stress-strain relations for dry and saturated sands, Part I, Incremental model, *Journal of Theoretical and Applied Mechanics*, 48, 2, 309–328.
- [41] Sawicki A., Świdziński W. (2010b), Stress-strain relations for dry and saturated sands, Part II, Predictions, *Journal of Theoretical and Applied Mechanics*, vol. 48, 2, 329–343.
- [42] Sławińska J. (2015), A modeling of pre-failure phenomena of granular soils, PhD thesis, IBW PAN.
- [43] Sumelka W. (2014), Application of fractional continuum mechanics to rate independent plasticity, *Acta Mechanica*, 225, 11, 3247–3264.
- [44] Sumelka, W. (2016), Fractional calculus for continuum mechanics—anisotropic non-locality, *Bull. Pol. Acad. Sci. Tech. Sci.* 64, 2, 361–372
- [45] Sun Y., Xiao Y. (2017), Fractional order plasticity model for granular soils subjected to monotonic triaxial compression, *International Journal of Solids and Structures*, 118-119, 224-234
- [46] Sun Y., Gao Y., Zhu Q. (2018), Fractional order plasticity modelling of state-dependent behaviour of granular soils without using plastic potential, *International Journal of Plasticity*, 102, 53-69.
- [47] Świdziński W. (2006), *Compaction and Liquefaction Mechanisms of Non-Cohesive Soils*, IBW PAN, Gdańsk (in Polish).
- [48] Świdziński W., Mierczyński J. (2005), Instability line as a basic characteristic of non-cohesive soils, *Archives of Hydro-Engineering and Environmental Mechanics*, 52, 1, 59-85.
- [49] Wood D. M. (1990), *Soil behaviour and critical state soil mechanics*, Cambridge University Press, New York/Part Chester/Melbourne/Sydney.
- [50] Atkinson J. (2007), *The mechanics of soils and foundations*, Taylor & Francis, London/New York.
- [51] Ziegler H. (1977), *An introduction to thermomechanics*, North Holland, Amsterdam.
- [52] Collins IF, Houslsby GT.(1997), Application of thermomechanical principles to the modelling of geotechnical materials. Proceedings of the Royal Society of London, Series A, 453, 1975–2001.
- [53] Houslsby GT, Puzrin AM. (2000), A thermomechanical framework for constitutive models for rate-independent dissipative materials, *International Journal of Plasticity*, 16(9), 1017–1047.
- [54] Kolymbas (2000), *Introduction to Hypoplasticity*, Taylor & Francis, London/New York.